Large eddy simulations of passive and buoyant scalars with dynamic subgrid-scale models

By W. Cabot

1. Motivations and objectives

Many flows of interest — especially those occurring in geophysical and astrophysical settings — have very high Reynolds numbers and, therefore, large dynamic ranges that cannot be captured by direct numerical simulation (DNS), even on today's supercomputers. Large eddy simulation (LES) is thus required, in which the large scale structures are resolved and the effects of the small, unresolved "subgrid" scales on the large, resolved scales are modeled.

A new subgrid-scale (SGS) model has recently been developed by Germano *et al.* (1991) that augments the standard Smagorinsky (1963) eddy viscosity model by replacing the *ad hoc*, flow-dependent constant with a coefficient extrapolated from the small, resolved scales in the LES. The coefficient automatically adjusts to the flow conditions, including near-wall conditions so that no *ad hoc* wall-damping functions are needed. This "dynamic" SGS model has been tested successfully by Germano *et al.* (1991) in the LES of incompressible channel flow with plane-averaged model coefficients, and the model has been extended to compressible flow by Moin *et al.* (1991).

The immediate goal of this work is to test the performance the dynamic SGS model and some of its possible variants in incompressible channel flow with passive scalars and with Boussinesq buoyancy. The LES results with the dynamic SGS model will be compared with low Reynolds number DNS data and with higher Reynolds number laboratory data. The consequences of implementing the dynamic SGS model at a local level rather than using globally averaged coefficients, which would be useful for applications with more complex geometries, will also be explored.

A longer range goal of this work will be to test the performance of SGS models in the LES of flows with more complicated physics (e.g., rotation and density stratification), applicable to geophysical and astrophysical systems.

2. Accomplishments

The basic dynamic SGS model for the residual Reynolds stress in LES was derived by Germano *et al.* (1991). The model was extended to compressible flow by Moin *et al.* (1991) and written explicitly for a passive scalar by Cabot & Moin (1991). A brief summary of the dynamic model equations and their variants are provided in §2.1 below for ready reference.

The dynamic SGS model for the passive scalar was evaluated *a priori* using DNS databases of homogeneous turbulence by Rogers *et al.* (1986) and channel flow by Kim & Moin (1989) to compute globally averaged SGS model coefficients. Results from these *a priori* tests were presented in detail in Moin *et al.* (1991) and Cabot

& Moin (1991). The key results from these tests are (1) the SGS turbulent Prandtl number of 0.4–0.5 predicted by the dynamic model away from solid boundaries in channel flow is about the same as that found to give the best performance in LES with standard eddy viscosity models (Eidson, 1985; Erlebacher *et al.*, 1990); and (2) the SGS turbulent Prandtl numbers predicted by the dynamic model follow the same trends as the large-scale Prandtl numbers near solid boundaries and for different molecular Prandtl numbers and orientations of scalar gradients with respect to the mean flow. This is an indication that the dynamic model in LES will predict reasonable values for the residual scalar transport.

A channel flow code described in detail by Piomelli *et al.* (1987) has been modified to include passive scalars and the dynamic SGS model with global coefficients (determined from plane-averaged terms). Low Reynolds number LES results for passive scalars generated by adding them at the bottom wall and removing them at the top wall have been compared to DNS data of J. Kim (personal communication) and Kim & Moin (1989); and LES results for a passive scalar generated by a uniform streamwise scalar gradient have been compared to DNS results of Kasagi *et al.* (1991). Nusselt numbers from these LES results and others at higher Reynolds numbers have been compared to the semi-empirical predictions of Kays & Crawford (1980). These results have been presented in Cabot & Moin (1991) and are summarized in §2.2.

This code has also been modified to simulate buoyant flows in the Boussinesq approximation, in which the scalar becomes the density fluctuation or, equivalently, the potential temperature. A low Rayleigh number case of Bénard convection has been simulated with the simple passive scalar dynamic SGS model, and higher Rayleigh number cases are under way. The results are being compared to the laboratory data of Deardorff & Willis (1967) and the LES results of Eidson (1985). Implementation of a dynamic version of a *buoyant* SGS model, like that used by Eidson, is discussed in §2.3.

The application of local SGS coefficients in the dynamic model is found to lead to numerical instability in this code (as well as in others), which is discussed in §2.4 below. The channel code of Kim *et al.* (1987), which is more generally robust in terms of numerical stability, has also been modified to include the local dynamic SGS model; numerical instability also arises in the LES using this code, apparently due to persistent regions of negative eddy viscosity.

2.1 The dynamic SGS model for passive scalars

In the LES of passive scalars, the residual Reynolds stress

$$\tau_{ij} = \overline{u_i u_j} - \overline{u_i}\,\overline{u_j} \tag{1a}$$

and the residual scalar flux

$$q_i = \overline{\theta u_i} - \overline{\theta}\,\overline{u_i} \tag{1b}$$

must be modeled. Here θ is the passive scalar, and u_i are the velocity components. The overbar denotes the filtering operation, which here shall always refer to a sharp cutoff filter in the homogeneous directions of the flow. Let τ_{ij} and q_i be modeled

by functions μ_{ij} and η_i. Further let the residual Reynolds stress and scalar flux at a coarser scale,

$$T_{ij} = \widehat{\overline{u_i}\,\overline{u_j}} - \widehat{\overline{u}_i}\,\widehat{\overline{u}_j}\,, \tag{2a}$$

$$Q_i = \widehat{\overline{\theta}\,\overline{u}_i} - \widehat{\overline{\theta}}\,\widehat{\overline{u}_i}\,, \tag{2b}$$

where the caret refers to the coarser "test" filter, be modeled similarly by M_{ij} and H_{ij}. Though neither the terms in (1) nor (2) are computable in the LES, the differences

$$\mathcal{L}_{ij} = T_{ij} - \hat{\tau}_{ij} = \widehat{\overline{u}_i\overline{u}_j} - \widehat{\overline{u}_i}\,\widehat{\overline{u}_j}\,, \tag{3a}$$

$$F_i = Q_i - \hat{q}_i = \widehat{\overline{\theta}\,\overline{u}_i} - \widehat{\overline{\theta}}\,\widehat{\overline{u}_i} \tag{3b}$$

are; hence

$$\mathcal{L}_{ij} = M_{ij} - \hat{\mu}_{ij}\,, \tag{4a}$$

$$F_i = H_i - \hat{\eta}_i\,. \tag{4b}$$

The Smagorinsky eddy viscosity model has the residual stress aligned with the strain rate S_{ij}:

$$\mu_{ij} = -2\nu_t\overline{S}_{ij}\,, \quad \nu_t = C\Delta^2|\overline{S}|\,, \tag{5a}$$

$$M_{ij} = -2\hat{\nu}_t\widehat{\overline{S}}_{ij}\,, \quad \hat{\nu}_t = C\widehat{\Delta}^2|\widehat{\overline{S}}|\,, \tag{5b}$$

where, generally,

$$2S_{ij} = u_{i,j} + u_{j,i}\,, \quad |S| \equiv (2S_{ij}S_{ij})^{1/2}\,; \tag{6}$$

and where Δ and $\widehat{\Delta}$ are the filter widths of the resolved field and the test filtered field, respectively, whose definitions will be discussed below. (Since the strain rate is traceless, this model strictly applies to the traceless part of the residual stress; in the incompressible equations, the trace of the residual stress is absorbed into the reduced pressure.) The residual scalar fluxes can be modeled similarly with an eddy diffusivity model in which they are aligned with the scalar gradients:

$$\eta_i = -\alpha_t\overline{\theta}_{,i}\,, \quad \alpha_t = C_\theta\Delta^2|\overline{S}|\,, \tag{7a}$$

$$H_i = -\hat{\alpha}_t\widehat{\overline{\theta}}_{,i}\,, \quad \hat{\alpha}_t = C_\theta\widehat{\Delta}^2|\widehat{\overline{S}}|\,. \tag{7b}$$

The coefficient C_θ is also expressed in terms of the SGS turbulent Prandtl number as C/Pr_t. Note too that the coefficients are assumed to be independent of the filter, which allows them to be determined algebraically in equations (4):

$$\mathcal{L}_{ij} - \mathcal{L}_{kk}\delta_{ij}/3 = -2C\Delta^2\mathcal{M}_{ij}\,, \quad \mathcal{M}_{ij} = (\widehat{\Delta}/\Delta)^2|\widehat{\overline{S}}|\widehat{\overline{S}}_{ij} - \widehat{|\overline{S}|\overline{S}_{ij}}\,, \tag{8a}$$

$$F_i = -C_\theta\Delta^2\mathcal{H}_i\,, \quad \mathcal{H}_i = (\widehat{\Delta}/\Delta)^2|\widehat{\overline{S}}|\widehat{\overline{\theta}}_{,i} - \widehat{|\overline{S}|\overline{\theta}_{,i}}\,. \tag{8b}$$

Other models for the residual Reynolds stress and scalar flux can of course be adopted.

Equations (8) are tensor and vector equations that overdetermine the scalar coefficients. The scalar coefficients were extracted by Germano *et al.* (1991) and Moin *et al.* (1991) by contracting (8a) with $\overline{S}_{ij}$ and (8b) with $\overline{\theta}_{,i}$ (the "strain-rate contraction"). Lilly (1991, private communication) suggested applying the least-squares technique to these equations, resulting in the contraction of (8a) with $\mathcal{M}_{ij}$ and (8b) with $\mathcal{H}_i$ (the "least-squares contraction"). LES results from channel flow using both contractions have been obtained with plane-averaging of the contracted quantities.

The filter width Δ is typically defined as the geometric ratio of the unidirectional filter widths Δ_i (Deardorff, 1970): $\Delta^3 = \Delta_1\Delta_2\Delta_3$. For a spectral cutoff wavenumber K_i, $\Delta_i = \pi/K_i$. However, since no explicit filtering occurs in the normal (y) direction in the channel LES code, it may be more appropriate to let $\Delta^2 = \Delta_1\Delta_3$. The dynamic eddy viscosity and diffusivity depend only on $\widehat{\Delta}/\Delta$, so that, for all $\widehat{\Delta}_i/\Delta_i$ the same, the former definition yields $\widehat{\Delta}/\Delta = (\widehat{\Delta}_i/\Delta_i)^{2/3}$ while the latter yields $\widehat{\Delta}/\Delta = \widehat{\Delta}_i/\Delta_i$ for channel flow. LES results using both definitions of filter width have been obtained and compared.

2.2 LES of passive scalars

A LES channel code (see Piomelli *et al.*, 1987) was modified to include passive scalars and the dynamic SGS model. The code uses Fourier decomposition in the homogeneous streamwise (x) and spanwise (z) directions and central finite differencing in the normal (y) direction. Time advancement is performed semi-implicitly with the Adams-Bashford, Crank-Nicholson method. The pressure is calculated directly in the Navier-Stokes equation. The plane-averaged part of the eddy viscosity from the SGS model is integrated implicitly. The flow was filtered in the horizontal directions with $\widehat{\Delta}_1/\Delta_1 = \widehat{\Delta}_3/\Delta_3 = 2$, which was found to yield the best *a priori* test results by Germano *et al.* (1991), and the SGS coefficients were computed as functions of normal direction and time from plane-averages of tensor and vector contractions in equations (8).

Simulations were performed for passive scalars added at one wall and removed at the other with Prandtl numbers $Pr = \nu/\alpha$ (where ν and α are the molecular kinematic viscosity and scalar diffusivity) of 0.1, 0.71, and 2.0 for low friction Reynolds numbers ($Re_\tau \equiv u_\tau\delta/\nu \approx 150$, where u_τ is the friction velocity and δ the channel half-depth); the strain-rate contraction was used with $\widehat{\Delta}/\Delta = 2^{2/3}$. The integrations were performed on $32 \times 63 \times 64$ meshes. The results were compared with DNS data (J. Kim, personal communication; cf. Kim & Moin, 1989). It was found that the SGS model was generally too dissipative. The mean streamwise velocity was found to exceed the DNS values by 10% in the log layer (see Figure 1a); the mean scalar from the LES also exceeded the DNS values substantially (the more so the larger the Prandtl number; see Figure 1b). The Nusselt number is defined by Kays & Crawford (1980) as

$$Nu = (4\delta/\Theta_m)|\partial\theta/\partial y|_w\,, \tag{9}$$

where $\Theta_m = \langle\theta u\rangle_V/\langle u\rangle_V$ is the mass-averaged scalar ($\langle\rangle_V$ denoting a global average), and where the gradient of the scalar is evaluated at the wall. For $Pr = 0.1$, 0.71, and 2.0, $Nu = 7.4$, 21.0, and 35.2 for the LES and 7.2, 23.8, and 43.8 for

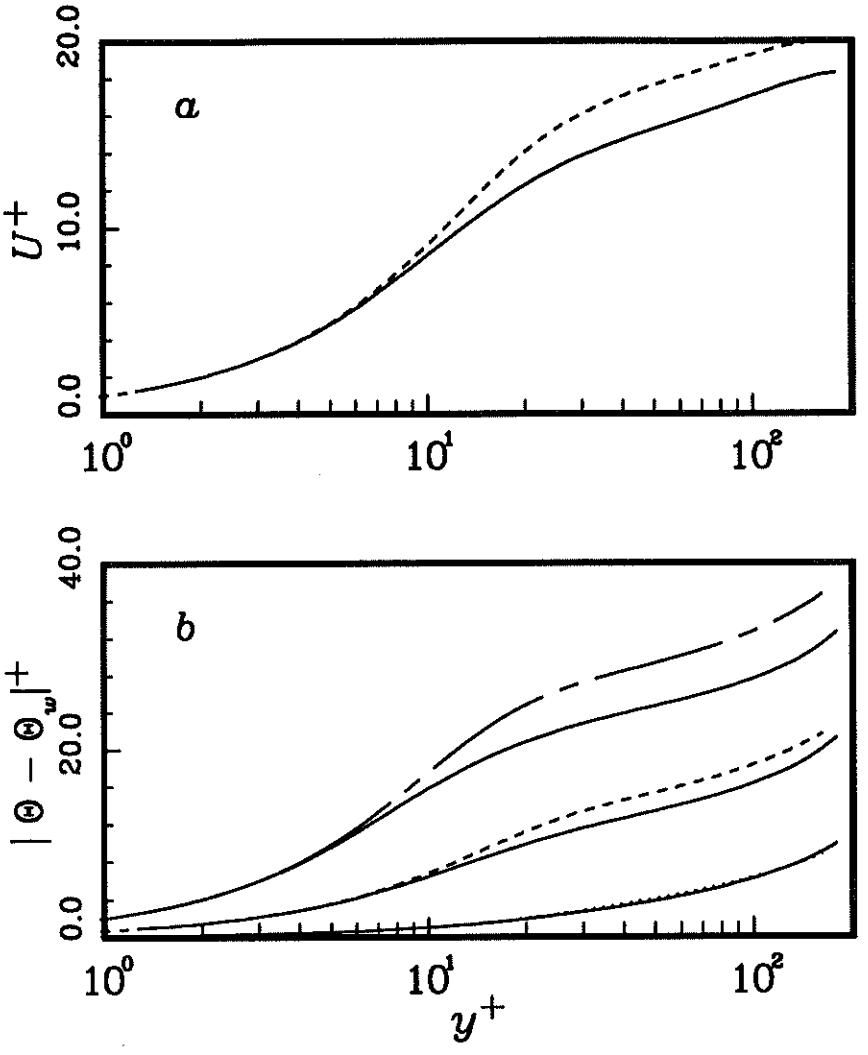

FIGURE 1. Mean profiles for low-Re LES with the strain-rate contraction and $\widehat{\Delta}/\Delta = 2^{2/3}$ (Case S1): (a) streamwise velocity (----) and (b) scalar for $Pr = 0.1$ (·····), 0.71 (----), and 2.0 (—-—); compared with the corresponding DNS data of J. Kim (personal communication) (———). Quantities are expressed in terms of wall ($^+$) units, i.e., scaled by δ, u_τ, and the scalar wall flux q_w.

the DNS, respectively, for the same mass-flux Reynolds number, $Re_m \equiv 4\delta\langle u\rangle_V/\nu$, of 1.12×10^4. The corresponding values predicted semi-empirically by Kays & Crawford are $Nu = 5.6$, 24.9, and 47.5, respectively. (These values were obtained from their Table 13-5 with a bilinear interpolation of $\log(Nu - Nu_o)$ in $\log Pr$ and $\log Re_m$, where Nu_o is the laminar value. Note that they express a lack of confidence in low-Pr values, and that the low-Pr values are also very sensitive to the interpolation scheme.)

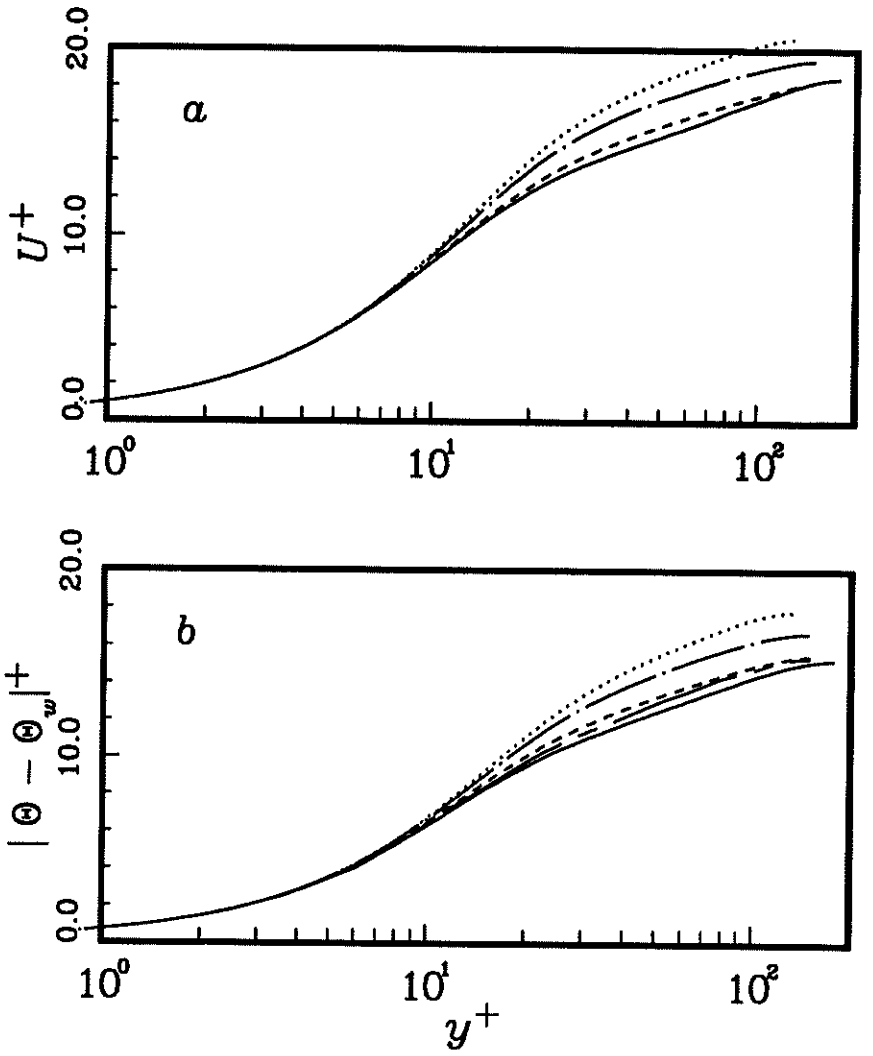

FIGURE 2. Mean profiles of (a) streamwise velocity and (b) $Pr = 0.71$ scalar for low-Re LES Cases S1 (·····), S2 (—·—), and M2 (- - - -) with a uniform streamwise scalar gradient. The DNS results of Kasagi *et al.* (1991) (——) for a uniform streamwise scalar gradient and those of Kim & Moin (1989) (———) for a uniform scalar source are shown for comparison.

Another set of low Reynolds number ($Re_\tau \approx 150$) simulations were performed with a passive scalar of $Pr = 0.71$ generated by a uniform streamwise scalar gradient, which gives very similar results to scalars generated by a uniform source term. Versions of the SGS model were used with the strain-rate contraction and $\widehat{\Delta}/\Delta = 2^{2/3}$ (Case S1) and $\widehat{\Delta}/\Delta = 2$ (Case S2), and with the least-squares contraction with $\widehat{\Delta}/\Delta = 2$ (Case M2); this sequence of models was found to give progressively less SGS dissipation (decreasing by an overall factor of 2). The mean

streamwise velocity and scalar are shown from these calculations in Figure 2 and compared with the recent DNS results of Kasagi *et al.* (1991) for a uniform streamwise scalar gradient and with the DNS results of Kim & Moin (1989) for a uniform scalar source term. It is evident that the less dissipative the SGS model, the better the agreement with the DNS data. The DNS results of Kasagi *et al.* had a Nusselt number of 30.8 for $Re_m = 9160$, or 9% lower than the value of $Nu = 34.0$ predicted by Kays & Crawford (1980). The values of Nu from the LES Cases S1, S2, and M2 were 31%, 22%, and 10% lower than predicted by Kays & Crawford, the lattermost case comparing very well with Kasagi *et al.*'s DNS results.

Simulations at much higher Reynolds number ($Re_\tau \approx 1400$ and $Re_m \approx 1.2 \times 10^5$) have been performed on a mesh of $32 \times 125 \times 64$ for a passive scalar of $Pr = 0.71$ added at the bottom wall and removed at the top wall. The SGS model with the strain-rate contraction and $\widehat{\Delta}/\Delta = 2^{2/3}$ (Case S1) was found to be much too dissipative and gave mean streamwise velocities about 25% too large compared to the standard empirical log law, $U^+ = 2.5 \ln y^+ + 5.0$, where y^+ is the distance from the wall in units of δ/Re_τ and U^+ is the mean streamwise velocity in units of friction velocity u_τ (see Figure 3a). Using the least-squares contraction gave much better results, with the less dissipative model with $\widehat{\Delta}/\Delta = 2$ (Case M2) performing somewhat better than with $\widehat{\Delta}/\Delta = 2^{2/3}$ (Case M1) (see Figure 3). The Nusselt number for Case S1 is 20% below that predicted by Kays & Crawford (1980), Nu for Case M1 is 3% higher, and Nu for Case M2 is 12% higher. The empirical curve for the mean scalar by Kader (1981) is shown for comparison in Figure 3b. Case M2 is seen to have about the same level as Kader's in the scalar log-law region, albeit with a slightly different slope. The large discrepancy at large y^+ near midchannel is because Kader's curve applies to scalars with uniform heating.

Note the occurrence of a bump in the mean streamwise velocity between $y^+ = 20$ and 200 above the standard log law in Figure 3a; the reason for this discrepancy is not yet known. Note, though, that this region where U^+ exceeds the log law actually agrees well with the DNS results of Kim *et al.* (1987), who used $U^+ = 2.5 \ln y^+ + 5.5$ to fit their data; this concordance may be coincidental, however. Another problem with the high Reynolds number simulation is the very short timesteps — and large amount of CPU and real time — that are necessary to achieve statistical equilibrium because of the refined mesh needed to resolve the wall layer; the convective CFL number is greatest in the region between the viscous layer and the log layer. Some sort of scheme for matching to the near-wall region, such as those used in the LES of planetary boundary layers, may be necessary to increase the speed of the LES at high Reynolds numbers for practical application.

2.3 LES of buoyant flows

The same LES channel code used in §2.2 above was also modified to calculate buoyant flows in the Boussinesq approximation (cf. Townsend, 1976). At present, the SGS model in this code is the same as that used for passive scalars described in §2.1 above. Simulations of Bénard convection (with the bottom wall heated and top wall cooled) are being performed for Rayleigh numbers ($Ra = 8\delta^3 \beta \Delta\Theta / \nu\alpha$, where $\beta_i = -\beta \delta_{i2}$ is the gravity vector times the expansion coefficient and $\Delta\Theta$ is

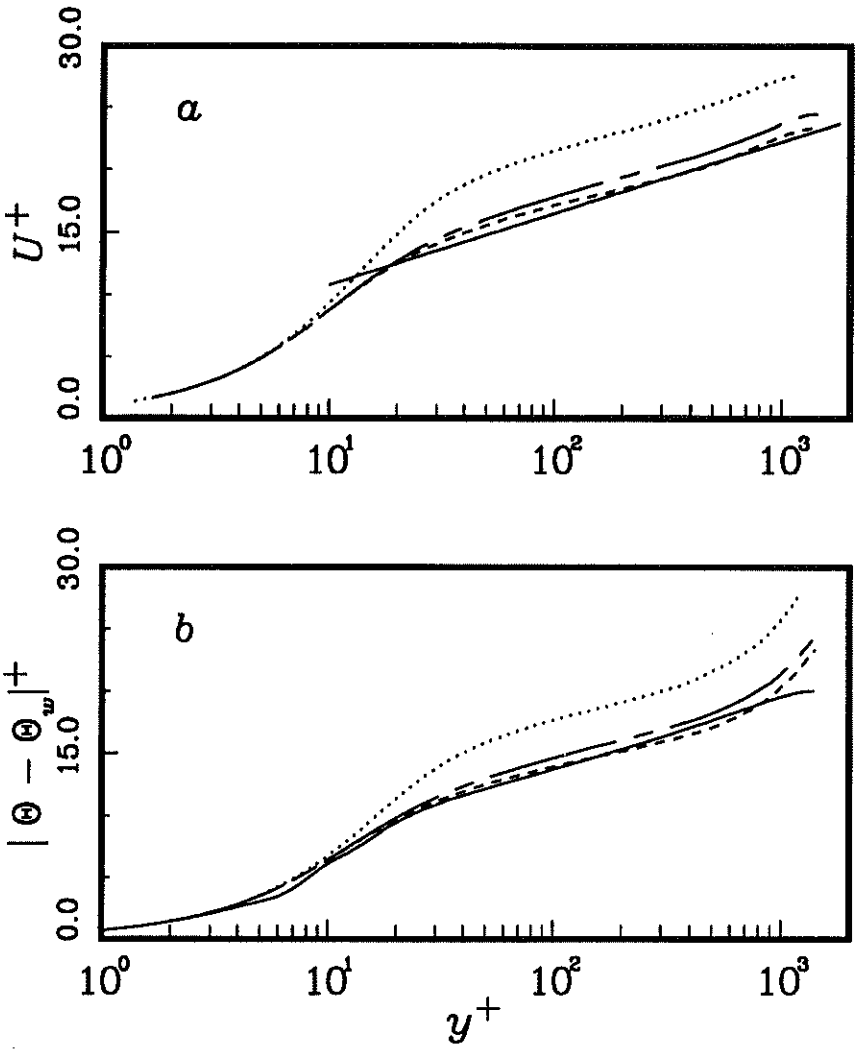

FIGURE 3. Mean profiles of (a) streamwise velocity and (b) $Pr = 0.71$ scalar for high-Re LES Cases S1 (·····), M1 (—·—), and M2 (- - - -). The log law, $U^+ = 2.5 \ln y^+ + 5.0$, is shown (———) in (a) for comparison. The empirical formula of Kader (1981) is shown (———) in (b) for $Re_\tau = 1400$ and $Pr = 0.71$.

the potential temperature difference across the channel) of 6.3×10^5, 2.5×10^6, and 1.0×10^7. Preliminary results give Nusselt numbers, defined here as $Nu = 2|\partial\theta/\partial y|_w \delta/\Delta\Theta$, of 7.5 and 12.0 for $Ra = 6.3 \times 10^5$ and 2.5×10^6, which lie between the LES values of about 9.5 and 13.8 found by Eidson (1985) and the laboratory values of about 6.0 and 8.0 found by Deardorff & Willis (1967). The eddy viscosity ν_t from the SGS model was found to be negative in the viscous wall region for $Ra = 6.3 \times 10^5$ (but very much smaller in magnitude there than the molecular viscosity); in the $Ra = 2.5 \times 10^6$ simulation, ν_t has negative values near the wall in

some realizations, but when averaged over time has positive mean values.

Many researchers who simulate buoyant flows feel that better results are obtained with the inclusion of a buoyancy production term in the SGS model (derived, e.g., by Eidson, 1985); the resulting model is, instead of (5) and (7),

$$\mu_{ij} = -2\nu_t \overline{S}_{ij}\,, \quad \nu_t = C\Delta^2\overline{\sigma}\,, \tag{10a}$$

$$M_{ij} = -2\widehat{\nu}_t \widehat{\overline{S}}_{ij}\,, \quad \widehat{\nu}_t = C\widehat{\Delta}^2\widehat{\overline{\sigma}}\,, \tag{10b}$$

and

$$\eta_i = -\alpha_t \overline{\theta}_{,i}\,, \quad \alpha_t = C_\theta \Delta^2 \overline{\sigma}\,, \tag{11a}$$

$$H_i = -\widehat{\alpha}_t \widehat{\overline{\theta}}_{,i}\,, \quad \widehat{\alpha}_t = C_\theta \widehat{\Delta}^2 \widehat{\overline{\sigma}}\,, \tag{11b}$$

where, generally,

$$\sigma = \left||S|^2 + N_c^2/Pr_t\right|^{1/2}\,, \quad N_c^2 \equiv \beta_i \theta_{,i} \tag{12}$$

is the new scaling factor. N_c is the convective lapse rate. For convectively stable regions $N_c^2 < 0$ (and $N = [-N_c^2]^{1/2}$ is the Brunt-Väisälä frequency), in which case the buoyancy production and the N_c^2 term in (12) are usually assumed to vanish, and the passive scalar SGS model is recovered. The dynamic model is now given by

$$\mathcal{L}_{ij} - \mathcal{L}_{kk}\delta_{ij}/3 = -2C\Delta^2 \mathcal{M}_{ij}\,, \quad \mathcal{M}_{ij} = (\widehat{\Delta}/\Delta)^2 \widehat{\overline{\sigma}}\widehat{\overline{S}}_{ij} - \widehat{\overline{\sigma}\overline{S}_{ij}}\,, \tag{13a}$$

$$F_i = -(C/Pr_t)\Delta^2 \mathcal{H}_i\,, \quad \mathcal{H}_i = (\widehat{\Delta}/\Delta)^2 \widehat{\overline{\sigma}}\widehat{\overline{\theta}}_{,i} - \widehat{\overline{\sigma}\overline{\theta}}_{,i}\,. \tag{13b}$$

The first complication that arises with this set of equations is the mode of contraction to extract C and Pr_t. A least-squares analysis leads to a messy and ambiguous result in the sense that one cannot even guarantee that one is minimizing the error! Therefore, in continuity with the previous least-squares contraction, let the error be minimized in the tensor and vector equations (13) with respect to only C, which again results in a contraction with $\mathcal{M}_{ij}$ and $\mathcal{H}_i$. Only SGS coefficients that are functions of y and t derived from plane-averages (denoted by $\langle\rangle$) of the contracted quantities will be considered here; thus

$$2C\Delta^2\langle \mathcal{M}_{ij}\mathcal{M}_{ij}\rangle = -\langle \mathcal{L}_{ij}\mathcal{M}_{ij}\rangle\,, \tag{14a}$$

$$C\Delta^2\langle \mathcal{H}_i\mathcal{H}_i\rangle = -Pr_t\langle F_i\mathcal{H}_i\rangle\,, \tag{14b}$$

where the contracted terms are functions of Pr_t. Even with this simple contraction, extracting the SGS coefficients presents a second complication since Pr_t is embedded in square roots in the σ terms. Eliminating C from (14b) gives

$$Pr_t\langle F_i\mathcal{H}_i\rangle\langle 2\mathcal{M}_{jk}\mathcal{M}_{jk}\rangle - \langle \mathcal{H}_i\mathcal{H}_i\rangle\langle \mathcal{L}_{jk}\mathcal{M}_{jk}\rangle = 0\,, \tag{15}$$

which is an expression solely in terms of Pr_t. This equation can be solved for Pr_t iteratively (e.g., by Newton's method), which can then be substituted into (14a)

to extract C. This procedure has been followed in *a priori* tests of DNS data for internally heated thermal convection in a channel (cf. Cabot *et al.*, 1990); the derivative of the function on the left side of (15) with respect to Pr_t, necessary to compute the correction in the Newton's method, was computed by numerical finite difference. In most planes, the procedure produced well converged solutions in only a few iterations, but in many planes the solution took more than 10 iterations to converge, and in rare instances no solution could be found at all (implying either complex solutions or problems with the numerical scheme). Multiple solutions also cannot generally be ruled out. Some further refinement and optimization of this iteration procedure is required in order to attain a more efficient version of it for use in the LES channel code.

A sample of *a priori* results from the DNS of the internally heated, buoyant channel flow (which is convectively stable in about the lower quarter of the channel and unstable elsewhere) are shown in Figure 4, comparing SGS coefficients with and without the buoyancy production term in (12). The DNS was performed on a mesh with 128 points (64 wavenumbers) in both horizontal directions; the coefficients shown in Figure 4 were computed for the same field on a "fine" mesh (using 32 and 16 wavenumbers for the resolved and test fields) and a "coarse" mesh (16 and 8 wavenumbers for the resolved and test fields). The coefficients from the fine field show little effect of the buoyancy production term, except near the upper wall where the buoyancy production is maximal. The effect the buoyancy production term on the SGS coefficients is much more evident in upper half plane using the coarser field, which would be more likely be the resolution used in a LES of this flow.

2.4 Numerical instability of the local dynamic SGS model

In order for the SGS model coefficients C and C_θ in (5) and (7) to be determined by (8), they must, in strict terms, be independent of the test filter or, more generally, be spatially independent of the directions in which filtering takes place. This is properly satisfied in the channel flow for coefficients that depend on only y and t determined from plane-averages. However, in order to extend the dynamic SGS model based on eddy viscosity and diffusivity to a more local definition that is more applicable complex geometries, this condition of self-consistency has been relaxed, and we have considered local values of the SGS model coefficients determined from equations (8). There is no obvious way yet to construct a *self-consistent* local eddy viscosity using the dynamic SGS model approach.

Germano *et al.* (1990) noted early on that the strain-rate contraction of (8a) leads to an ill-conditioned local problem due to the denominator term $\mathcal{M}_{ij}\overline{S}_{ij}$ frequently traversing zero. The least-squares contraction in principle solves this problem, since one is now dividing by $\mathcal{M}_{ij}\mathcal{M}_{ij}$ and $\mathcal{H}_i\mathcal{H}_i$, which are positive definite. *A priori* test of DNS channel flow data has shown that this problem is still not very well conditioned, because the denominators occasionally (perhaps as much as 1% of the time) become very small, leading to large local spikes in the coefficients. Further, the numerators ($\mathcal{L}_{ij}\mathcal{M}_{ij}$ and $F_i\mathcal{H}_i$) exhibit the usual backscatter statistics, with roughly half of the points being positive and the other half being negative (cf. Piomelli *et al.*, 1991). The result is local eddy viscosities and diffusivities that have

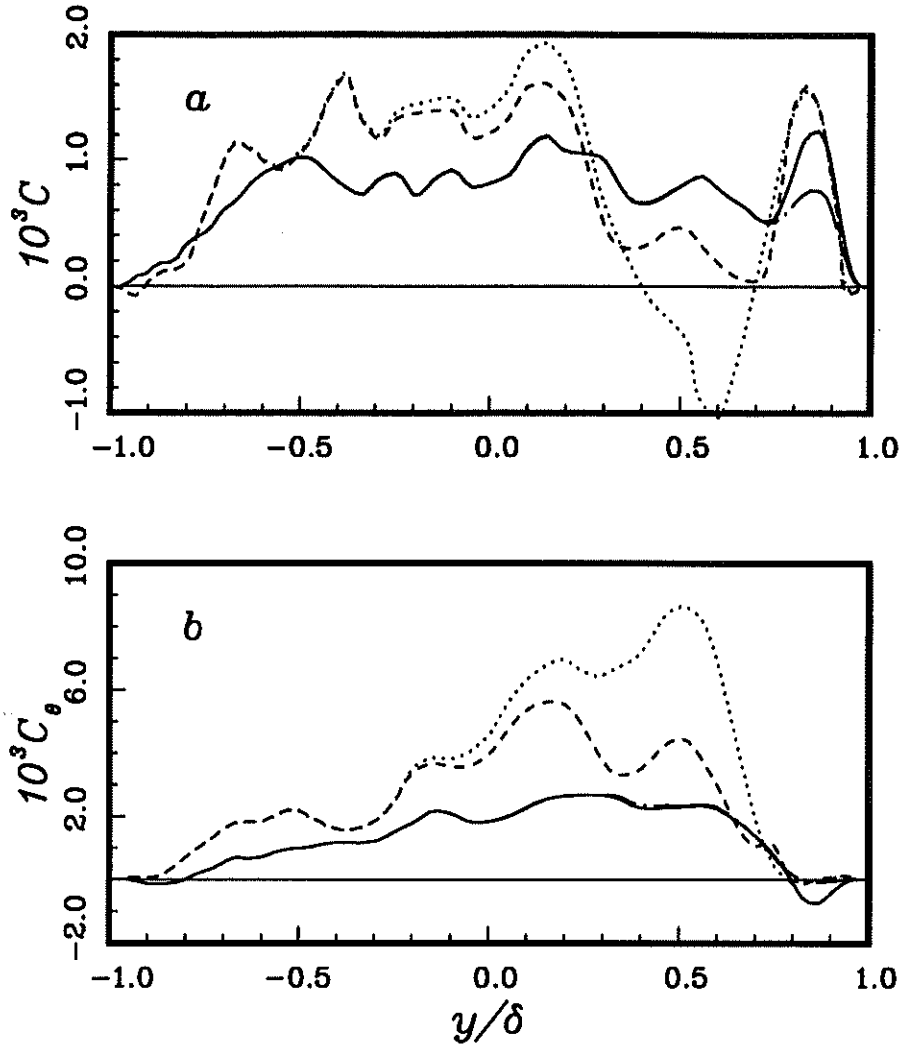

FIGURE 4. The (global) dynamic SGS (a) velocity and (b) scalar coefficients from *a priori* tests of DNS data for an internally heated, buoyant channel flow with $Ra = 1.25 \times 10^5$ and $Pr = 0.04$. The coefficients were computed using equations (14) and (15) *without* the buoyancy production term in (12) on a fine mesh (—·—) and coarse mesh (·····), and *with* the buoyancy production term on the fine mesh (———) and coarse mesh (- - - -).

r.m.s. values much larger than (5–10 times) the mean values (which is expected), but extrema that are often 100 times the r.m.s. values. Local spatial averaging or filtering (over scales a few times the resolved scales, say) ameliorates the spikiness of the local results, but only by factors of a few.

Some preliminary *a priori* tests were conducted exploring whether some of the ill behavior of the local eddy viscosities and diffusivities were due to an inappropriate

model which seeks to align the residual stresses and scalar fluxes with strains and scalar gradients. One model (P. Durbin, personal communication) uses a second-rank tensor SGS coefficient C_{ij}, such that

$$\tau_{ij} = -(C_{ik}\overline{S}_{kj} + C_{jk}\overline{S}_{ki})\Delta^2|\overline{S}|, \tag{16a}$$

$$T_{ij} = -(C_{ik}\widehat{\overline{S}}_{kj} + C_{jk}\widehat{\overline{S}}_{ki})\widehat{\Delta}^2|\widehat{\overline{S}}|, \tag{16b}$$

such that, instead of (8a),

$$\mathcal{L}_{ij} = -(C_{ik}\mathcal{M}_{kj} + C_{jk}\mathcal{M}_{ki})\Delta^2; \tag{17}$$

but this model also turns out to be ill-conditioned, since it involves dividing by the determinant of $\mathcal{M}$, which frequently traverses zero. A more general model should use a fourth-rank tensor for C and a second-rank tensor for C_θ (which Rogers *et al.*, 1986, found to be appropriate for the large-scale scalar fluxes). Another model that was tested locally included the second-order strain term, such that

$$\tau_{ij} - \tau_{kk}\delta_{ij}/3 = -2C_1\Delta^2|\overline{S}|\overline{S}_{ij} - 2C_2\Delta^2(\overline{S}_{ik}\overline{S}_{kj} - \overline{S}_{k\ell}\overline{S}_{\ell k}\delta_{ij}/3), \tag{18}$$

and so on. The least-squares analysis for C_1 and C_2 leads to the inversion of a matrix, whose determinant again traverses zero frequently and thus leads to ill-conditioned results. More sophisticated models that attempt to align the residual stress to a more appropriate basis are currently being explored by T. S. Lund (this volume).

The local dynamic SGS model (using equations [8] and some variants) was used in the channel code described in §2.2. The code very quickly developed large normal pressure oscillations (resembling "2-Δ" waves) that caused the simulations to blow up. It had been noticed previously that this code was unstable to sufficiently choppy data, perhaps due to the direct computation of the pressure in the Navier-Stokes equation and/or due to the central finite difference scheme employed. A more stable channel code (see Kim *et al.*, 1987) has recently been modified to include the dynamic SGS model with plane-averaged or local coefficients; this code uses Chebyshev decomposition in the direction normal to the walls and solves the Navier-Stokes equation in a form that has the pressure eliminated from it. The SGS residual Reynolds stress and scalar flux are integrated fully explicitly, and the CFL condition due to the SGS diffusion is monitored (which generally limits the timestep for local SGS coefficients due to their inherently large maxima). A simulation with plane-averaged SGS coefficients was performed and experienced no instabilities. When the local model (from [8]) was employed, the SGS dissipation quickly changed sign from a damping state to a growing state (corresponding to a build-up of local negative eddy viscosity), and the calculation blew up. The simulation did not, however, exhibit the wild pressure oscillations characteristic of the previous finite-difference code. Similar instabilities were observed for various degrees of local averaging or filtering, despite a reduction in the r.m.s. and extremal

levels of eddy viscosity/diffusivity. Similar instabilities were also observed using variants of the model in (5) and (7): in one, the mean strain rate and scalar gradient were excluded from the definitions, similar to that used by Moin & Kim (1982); and in another only the last octave of wavenumbers at a given filter level were used to compute $|S|$. The numerical instability apparently arises from regions of negative eddy viscosity that persist long enough with respect to the integration timesteps to cause the calculation to diverge exponentially.

Another local dynamic SGS model was attempted, which *is* locally self-consistent but not *per se* an eddy viscosity/diffusivity model, namely making the residual stress and scalar flux proportional to their counterparts in (3) with scaling factors:

$$\tau_{ij} = \mathcal{L}_{ij}\left(\Delta^2|\overline{S}|^2 \Big/ \widehat{\Delta}^2|\widehat{\overline{S}}|^2\right), \tag{19a}$$

$$q_i = F_i\left(\Delta^2|\overline{S}||\nabla\overline{\theta}| \Big/ \widehat{\Delta}^2|\widehat{\overline{S}}||\nabla\widehat{\overline{\theta}}|\right). \tag{19b}$$

A priori tests indicate that this model should be dissipative (in the mean). In this LES, the SGS model dissipation also went from damping to growing, causing the simulation to blow up in a similar time as the local eddy viscosity models. The reason for the numerical instability is likely the same — with persistent regions of "backscatter" experiencing runaway growth — although an analogy with negative viscosities is no longer exact.

3. Future plans

Further testing of the dynamic SGS model for passive scalars with global (plane-averaged) coefficients in the LES in channel flow will continue. In particular, the performance of SGS models that use the fluctuating part of the strain rate tensor (à la Kim & Moin, 1982) will be tested. Also at issue with the high Reynolds number simulations is (1) explaining the deviation from the log law observed in the mean streamwise velocity profile; and (2) exploring means to increase the integration timesteps in the simulations (e.g., using near-wall matching conditions).

Much more extensive testing of the dynamic model for buoyant flows will be performed. The sequence of simulations of Bénard convection discussed in §2.3 will be completed and compared in detail to the laboratory and LES results; in particular the SGS model that includes the buoyancy production terms will be implemented, and it will be determined if its added computational costs are worth the benefits, if any, it confers. The LES of Bénard convection at somewhat higher Rayleigh numbers (near the "hard turbulence" régime) will be attempted and compared to laboratory results (e.g., Heslot *et al.*, 1987) of statistical quantities like Nusselt number and vertical velocity-temperature correlations. The LES of internally heated, buoyant flow will also be performed for different versions of the dynamic SGS model and compared to laboratory results (e.g., Kulacki & Goldstein, 1972) and numerical simulation results (e.g., Grötzbach, 1982).

The performance of the dynamic SGS model in the presence of rotation will also be explored, in particular whether the model can automatically take account of the

observed rotational inhibition of the turbulent transfer of energy to small scales (Bardina *et al.*, 1985) within the framework of a simple eddy viscosity model, or if additional modeling terms are needed. The effects of differential rotation will also be considered. DNS data from uniformly and differentially rotating buoyant flows will be used for comparison (e.g., Cabot *et al.*, 1990; Cabot & Pollack, 1991). An important, ultimate application of a successfully developed and tested SGS model will be in the LES of large Reynolds number geophysical and astrophysical flows with differential rotation, thermal convection, large density stratification, and perhaps other compressibility effects.

Finally, the dynamic SGS model has only been successfully employed with *global* eddy viscosity and diffusivity coefficients, which limits its application to flows with a large degree of homogeneity. A model that uses locally determined coefficients would have more universal applicability to geometrically complex flows. Considerable effort will be devoted to removing this deficiency.

REFERENCES

BARDINA, J., FERZIGER, J. H., & ROGALLO, R. S. 1985 Effect of rotation on isotropic turbulence: Computation and modeling. *J. Fluid Mech.* **154**, 321–336.

CABOT, W., HUBICKYJ, O., POLLACK, J. B., CASSEN, P., & CANUTO, V. M. 1990 Direct numerical simulations of turbulent convection: I. Variable gravity and uniform rotation. *Geophys. Astrophys. Fluid Dyn.* **53**, 1–42.

CABOT, W., & MOIN, P. 1991 Large eddy simulation of scalar transport with the dynamic subgrid-scale model. In *Large Eddy Simulation of Complex Engineering and Geophysical Flows*, ed. by B. Galperin, in press. Cambridge University Press.

CABOT, W., & POLLACK, J. B. 1991 Direct numerical simulations of turbulent convection: II. Variable gravity and differential rotation. *Geophys. Astrophys. Fluid Dyn.*, in press.

DEARDORFF, J. W. 1970 A numerical study of three-dimensional turbulent channel flow at large Reynolds numbers. *J. Fluid Mech.* **41**, 453–480.

DEARDORFF, J. W., & WILLIS, G. E. 1967 Investigation of turbulent thermal convection between horizontal plates. *J. Fluid Mech.* **28**, 675–704.

EIDSON, T. M. 1985 Numerical simulation of turbulent Rayleigh-Bénard convection using subgrid scale modeling. *J. Fluid Mech.* **158**, 245–268.

ERLEBACHER, G., HUSSAINI, M. Y., SPEZIALE, C. G., & ZANG, T. A. 1990 Toward the large-eddy simulation of compressible turbulent flows. *ICASE Rep. 90-76.* ICASE & NASA/Langley Research Center.

GERMANO, M., PIOMELLI, U., MOIN, P., & CABOT, W. H. 1991 A dynamic subgrid-scale eddy viscosity model. *Phys. Fluids A.* **3**, 1760–1765.

GRÖTZBACH, G. 1982 Direct numerical simulation of the turbulent momentum and heat transfer in an internally heated fluid layer. In *Heat Transfer 1982*, vol. 2,

ed. by U. Grigull, E. Hahne, K. Stephan & J. Straub, pp. 141–146. Hemisphere Publishing.

HESLOT, F., CASTAING, B., & LIBCHABER, A. 1987 Transitions to turbulence in helium gas. *Phys. Rev. A.* **36**, 5870–5873.

KADER, B. A. 1981 Temperature and concentration profiles in fully turbulent boundary layers. *Int. J. Heat Mass Trans.* **24**, 1541–1544.

KASAGI, N., TOMITA, Y., & KURODA, A. 1991 Direct numerical simulation of passive scalar field in a two-dimensional turbulent channel flow. *ASME J. Heat Trans.*, in press.

KAYS, W. M., & CRAWFORD, M. E. 1980 *Convective Heat and Mass Transfer*, 2nd ed., ch. 13. McGraw-Hill.

KIM, J., & MOIN, P. 1989 Transport of a passive scalar in a turbulent channel flow. In *Turbulent Shear Flows 6*, ed. by J.-C. André, J. Cousteix, F. Durst, B.E. Launder, F.W. Schmidt, & J.H. Whitelaw, pp.86–96. Springer-Verlag.

KIM, J., MOIN, P., & MOSER, R. 1987 Turbulence statistics in fully developed channel flow at low Reynolds number. *J. Fluid Mech.* **177**, 133–166.

KULACKI, F. A., & GOLDSTEIN, R. J. 1972 Thermal convection in a horizontal fluid layer with uniform volumetric energy sources. *J. Fluid Mech.* **55**, 271–287.

MOIN, P., & KIM, J. 1982 Numerical investigation of turbulent channel flow. *J. Fluid Mech.* **118**, 341–377.

MOIN, P., SQUIRES, K., CABOT, W., & LEE, S. 1991 A dynamic subgrid-scale model for compressible turbulence and scalar transport. *Phys. Fluids A.* **3**, 2746–2757.

PIOMELLI, U., CABOT, W. H., MOIN, P., & LEE, S. 1991 Subgrid-scale backscatter in transitional and turbulent flows. *Phys. Fluids A.* **3**, 1766–1771.

PIOMELLI, U., FERZIGER, J. H., & MOIN, P. 1987 Models for large eddy simulations of turbulent channel flows including transpiration. *Rep. TF-32, Dept. of Mech. Eng.* Stanford University.

ROGERS, M., MOIN, P., & REYNOLDS, W. C. 1986 The structure and modeling of the hydrodynamic and passive scalar fields in homogeneous turbulent shear flow. *Rep. TF-25, Dept. of Mech. Eng.* Stanford University.

SMAGORINSKY, J. 1963 General circulation experiments with the primitive equations. I. The basic experiment. *Mon. Weather Rev.* **91**, 99–164.

TOWNSEND, A. A. 1976 *The Structure of Turbulent Shear Flow*, 2nd ed., ch. 2. Cambridge University Press.